Quaternary Science Reviews 162 (2017) 60–71

Contents lists available at ScienceDirect

Quaternary Science Reviews

journal homepage: www.elsevier.com/locate/quascirev

Dust composition changes from Taylor Glacier (East Antarctica) during the last glacial-interglacial transition: A multi-proxy approach

Sarah M. Aarons [a, *], Sarah M. Aciego [a], Carli A. Arendt [a, 1], Molly A. Blakowski [a], August Steigmeyer [a], Paolo Gabrielli [b, c], M. Roxana Sierra-Hernández [b], Emilie Beaudon [b], Barbara Delmonte [d], Giovanni Baccolo [d, e], Nathaniel W. May [f], Kerri A. Pratt [f, a]

[a] Department of Earth and Environmental Sciences, University of Michigan, 1100 N. University Avenue, Ann Arbor, MI, 48109-1005, USA
[b] Byrd Polar and Climate Research Center, The Ohio State University, 108 Scott Hall, 1090 Carmack Road, Columbus, OH, 43210, USA
[c] School of Earth Science, The Ohio State University, 275 Mendenhall Laboratory, 125 South Oval Mall, Columbus, OH, 43210, USA
[d] Department of Environmental Science, University of Milano-Bicocca, Piazza della Scienza 1, Milan, 20126, Italy
[e] Graduate School in Polar Sciences, University of Siena, via Laterina 8, Siena, 53100, Italy
[f] Department of Chemistry, University of Michigan, 930 N. University Avenue, Ann Arbor, MI, 48109-1005, USA

ARTICLE INFO

Article history:
Received 2 December 2016
Accepted 8 March 2017
Available online 10 March 2017

Keywords:
Holocene
Pleistocene
Climate dynamics
Paleoclimatology
Antarctica
Ice cores
Radiogenic isotopes
Dust

ABSTRACT

Mineral dust is transported in the atmosphere and deposited in oceans, ice sheets and the terrestrial biosphere. Temporal changes in locations of dust source areas and transport pathways have implications for global climate and biogeochemical cycles. The chemical and physical characterization of the dust record preserved in ice cores is useful for identifying of dust source regions, dust transport, dominant wind direction and storm trajectories. Here, we present a 50,000-year geochemical characterization of mineral dust entrapped in a horizontal ice core from the Taylor Glacier in East Antarctica. Strontium (Sr) and neodymium (Nd) isotopes, grain size distribution, trace and rare earth element (REE) concentrations, and inorganic ion (Cl^- and Na^+) concentrations were measured in 38 samples, corresponding to a time interval from 46 kyr before present (BP) to present. The Sr and Nd isotope compositions of insoluble dust in the Taylor Glacier ice shows distinct changes between the Last Glacial Period (LGP in this study ranging from ~46.7–15.3 kyr BP) the early Holocene (in this study ranging from ~14.5–8.7 kyr BP), and zero-age samples. The $^{87}Sr/^{86}Sr$ isotopic composition of dust in the Taylor Glacier ice ranged from 0.708 to 0.711 during the LGP, while the variability during the early Holocene is higher ranging from 0.707 to 0.714. The ε_{Nd} composition ranges from 0.1 to −3.9 during the LGP, and is more variable from 1.9 to −8.2 during the early Holocene. The increased isotopic variability during the early Holocene suggests a shift in dust provenance coinciding with the major climate transition from the LGP to the Holocene. The isotopic composition and multiple physical and chemical constraints support previous work attributing Southern South America (SSA) as the main dust source to East Antarctica during the LGP, and a combination of both local Ross Sea Sector dust sources and SSA after the transition into the Holocene. This study provides the first high time resolution data showing variations in dust provenance to East Antarctic ice during a major climate regime shift, and we provide evidence of changes in the atmospheric transport pathways of dust following the last deglaciation.

1. Introduction

Ice cores drilled from the Greenland and Antarctic ice sheets are excellent archives of atmospheric composition and climate over hundreds of thousands of years (EPICA community members, 2004; Jouzel et al., 1997; Petit et al., 1999). Climate parameters, such as greenhouse gas (CO_2 and CH_4) concentrations, and climate proxies, such as stable isotope variability in precipitation, are utilized in ice

* Corresponding author. Department of Earth System Science, University of California, Irvine, 3200 Croul Hall Street, Irvine, CA, 92697, USA.
E-mail address: smaarons@uci.edu (S.M. Aarons).
[1] Current address: Los Alamos National Laboratory, Earth System Observations (EES-14), Atmosphere, Climate and Ecosystem Science Team, Los Alamos, New Mexico, 87544, USA.

http://dx.doi.org/10.1016/j.quascirev.2017.03.011
0277-3791/

cores to reconstruct long-term records of atmospheric change (Loulergue et al., 2008; Lüthi et al., 2008). Variations in dust fluxes to polar ice sheets during glacial-interglacial periods are correlated to proxies for temperature changes (reconstructed from δD and $\delta^{18}O$ records) over long timescales (Basile et al., 1997; Biscaye et al., 1997, and references therein). Physical and chemical characterization of dust particles deposited in Antarctic ice is used to trace fine-grained mineral material (dust) to its origins as sediment generated in potential source areas (PSAs) (Grousset and Biscaye, 2005, and references therein).

The dominant source of dust to East Antarctica during the Last Glacial Period (LGP in this study ranging from ~46.7–15.3 kyr BP) was most likely Southern South America (SSA) (Grousset et al., 1992; Vallelonga et al., 2010, and references therein). Higher amounts of dust were transported to Antarctica during glacial periods, relative to interglacial periods, due to increased dust availability at the source area and windier conditions caused by a more pronounced pole-equator temperature gradient (Hammer et al., 1985; Petit and Delmonte, 2009; Sugden et al., 2009). In contrast, dust transported to Antarctica during the early Holocene (in this study ranging from ~14.5–8.7 kyr BP) and present day is not well characterized from a geochemical perspective due to the extremely small concentrations preserved in Antarctic ice (Delmonte et al., 2010). The observation of larger dust particles in Holocene ice from coastal East Antarctic sites such as Talos Dome (Fig. 1, see inset) indicates a higher input of local (high-elevation ice-free

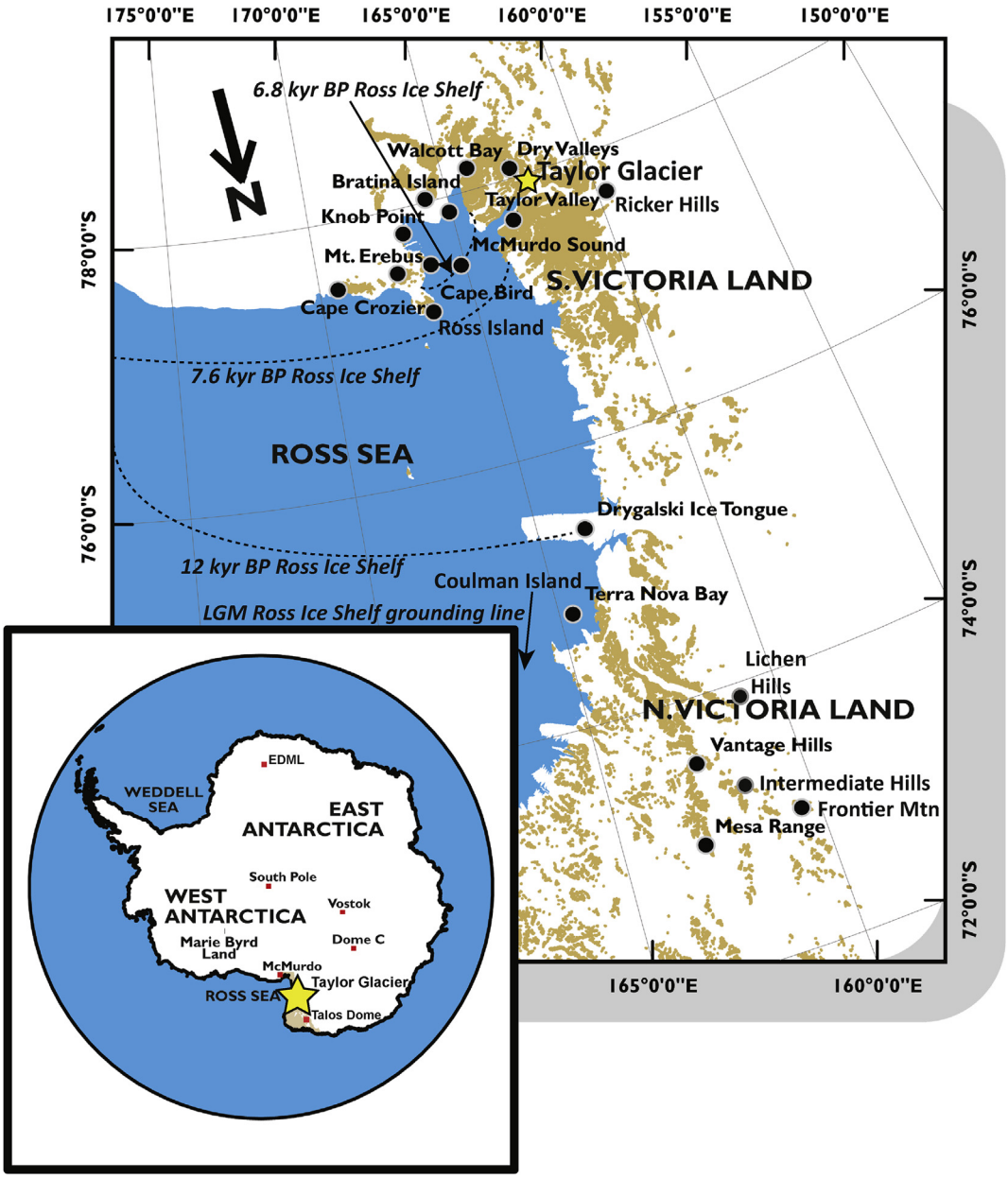

Fig. 1. Location map of Taylor Glacier and surrounding area. The East Antarctic Ice Sheet shaded in white, the Ross Sea in blue, and exposed rock surfaces in brown. Taylor Glacier (yellow star) is shown relative to potential source areas of dust and important landmarks (Drygalski ice tongue, Ross Island, and Coulman Island) discussed here. Dashed lines with age listed show the timing of the Ross Ice Shelf grounding line retreat (Licht et al., 1996; Conway et al., 1999). Inset map shows locations of Antarctic ice core drilling sites EDML, South Pole, Vostok, Dome C, Taylor Dome, and Taylor Glacier (yellow star). Figure adapted from Blakowski et al. (2016). (For interpretation of the references to colour in this figure legend, the reader is referred to the web version of this article.)

Antarctic terrains) rather than remote (SSA) dust sources (Delmonte et al., 2010). However, dust particles found in central East Antarctic ice cores remain fine (always <5 μm) during the Holocene, due to the constant input of dust from distal sources (Delmonte et al., 2002). However, isotopic (Sr-Nd composition; Revel-Rolland et al., 2006, lead (Pb) composition; Vallelonga et al., 2010) and elemental (rare earth elements (REE); Gabrielli et al., 2010; major elements; Marino et al., 2008) data show a shift in dust composition with respect to the LGP, suggesting an influence of sources other than (or in addition to) SSA (Revel-Rolland et al., 2006, and references therein).

Here we investigate the dust cycle in the Ross Sea region during the last climatic transition, from the LGP to the early Holocene. This is a critical region from a climatic perspective as most of the major components of the Antarctic climate system intersect here (i.e. the East and West Antarctic Ice Sheet, the Ross Sea Ice Shelf and the Southern Ocean). The intersection of the different Antarctic climate system components, in tandem with the presence of many ice-free sites throughout the region increase the complexity of the dust cycle in this portion of Antarctica (Albani et al., 2012; Delmonte et al., 2013; Aarons et al., 2016). In this study, a high-volume, multi-millennial horizontal ice core at Taylor Glacier was used to: 1) distinguish proximal versus distant dust sources; 2) determine if changes in climate in the Ross Sea region from the last glacial maximum (LGM, ~21 kyr BP) through the Preboreal Holocene is recorded by particle compositional changes; and 3) provide a record of Southern Hemisphere dust at a coastal Antarctic site through a major climate transition. Dust concentration and size distribution, trace and REE concentrations, inorganic ion concentrations, and radiogenic isotope composition of dust within the Taylor Glacier horizontal ice core are used to show the restructuring of sources and transport pathways of dust in this region during the last deglaciation. These records are integrated with the current understanding of climate in the Ross Sea region and a record from East Antarctica to understand the Antarctic dust record variation with large-scale climate transitions on glacial-interglacial timescales. In particular, understanding the changes in dust composition during a major climate transition provides insight into the relationship between atmospheric transport, increasing ambient temperatures, and large-scale ice shelf retreat.

2. Regional setting

Taylor Glacier is located on the eastern portion of the East Antarctic ice sheet (Fig. 1), close to the Ross Ice Shelf and the Ross Sea seasonal sea ice. Taylor Glacier ice originates from its point of accumulation at Taylor Dome (Bliss et al., 2011), and terminates on land in the McMurdo Dry Valleys. The ice surface is mostly smooth and crevasse free, but thermal contraction caused by variations in summer and winter temperatures results in surface cracking that may reach several meters below the surface. Katabatic-driven movements of cold air masses originating from interior Antarctica have a strong influence on the weather (Morse et al., 1998). These cold air masses approach primarily from the southwest (Morse et al., 1998), whereas warmer air masses with high amounts of precipitation approach from the south (Morse, 1997).

The extremely low dust concentrations coupled with limited ice available for measurements presents a major analytical limitation for ice core science. Traditional ice cores are expensive and logistically challenging to retrieve, and the small masses of ice recovered from any given depth places limitations on the quantity and variety of analytical measurements. Because of the extremely limited amount of dust present in Antarctic ice, especially during the Holocene, it is necessary to collect larger ice samples for more precise and accurate radiogenic isotope measurements. To overcome this obstacle, an alternative approach to traditional ice core collection was employed using ice exposed in the ablation area of a glacier.

Ice sheet dynamics result in the oldest ice exposed at the ablation area, or at the ice sheet margin as the ice flows outward from the accumulation area. The horizontal exposure of ice stratigraphy leads to the oldest ice at the toe of the glacier and progressively younger ice towards the equilibrium line. Ice exposed in this fashion has been referred to as a 'horizontal ice core,' and has been used successfully in previous paleoclimate studies (Aciego et al.,

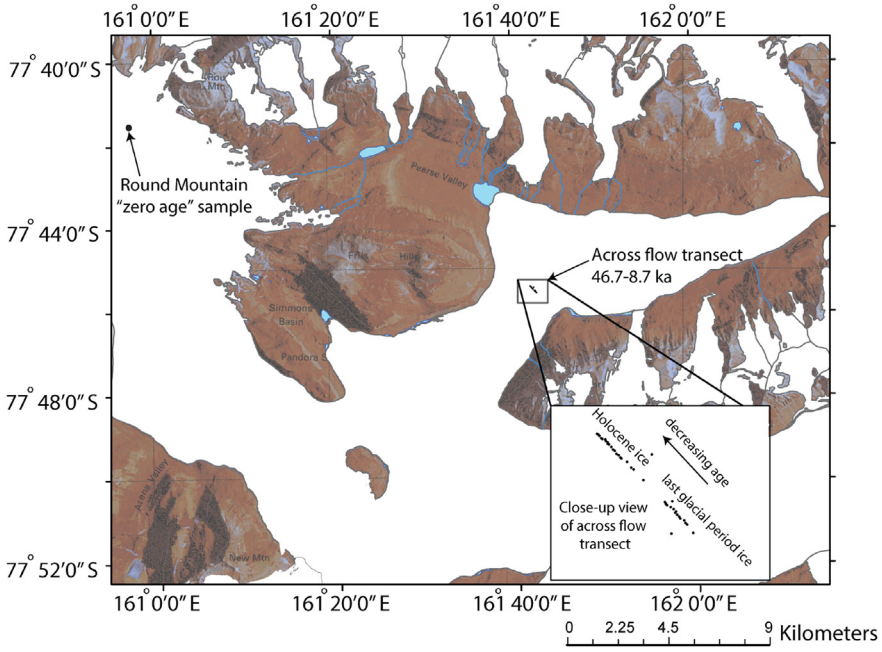

Fig. 2. Sampling transect locations (•) and the 'zero-age' sample at Round Mountain. Each symbol represents one sample. Inset map on right is a close up of the sampling transect and age relationship of sampling transect.

2007; Reeh et al., 1991), as well as for the acquisition of previously unobtainable measurements of trace gases, and isotopes of trace gases (Buizert et al., 2014; Petrenko et al., 2016). Previous work investigating trapped gas concentrations throughout the lower Taylor Glacier (Buizert et al., 2014; Petrenko et al., 2016) found an area of the glacier where a tight bend in the ice results in 40,000 yrs of ice exposure in an across glacier transect (Fig. 2). This perpendicular to ice flow 'horizontal ice core' drilled from Taylor Glacier, East Antarctica was used in this study to characterize the dust deposited during the LGP, the deglaciation, and the early Holocene.

2.1. Age scale of Taylor Glacier 'horizontal ice core'

Ice spanning a large range of ages (in this study from ~45 to 0 kyr BP) is present at the surface of Taylor Glacier, and any change in the ice age occurs either down the center ice flow line or perpendicular to the ice flow line (Aciego et al., 2007; Buizert et al., 2014). Baggenstos (2015) established the ice age of the Taylor Glacier across flow transect using trace gas measurements covering marine isotope stage (MIS) 3, the LGM, and the deglaciation into the Holocene. From this, an age model was created for the Taylor Glacier transect using CH_4 and CO_2 inflection points (Bauska, 2013) and the isotopic composition of atmospheric oxygen ($\delta^{18}O$ of O_2, or $\delta^{18}O_{atm}$) as additional tie points (Baggenstos, 2015). Because the ice stratigraphy of Taylor Glacier is folded with Holocene (spatial length of horizontal core transect: +30–260 m) ice on one side and LGP (−80 to −300 m) ice on the other side of the fold, two separate age models were developed for each side of the fold (Baggenstos, 2015). The resulting age models have an overlap of ~2000 years, and more details on the sample ice ages are presented in Table 1.

3. Materials and methods

3.1. Sample collection

The 'horizontal ice core' exposed at the Taylor Glacier surface was collected during a field season in the austral summer (November–December) 2013. Drilling was performed with the Blue Ice Drill (BID) (Kuhl et al., 2014) provided by Ice Drilling Design and Operations (IDDO). The BID retrieves ice cores that are 1 m in length and 24 cm in diameter, weighing ~40 kg. The 'horizontal ice core' (Fig. 2), consists of 119 samples (80 unique, 39 duplicate) spanning the time interval of ~46–8.7 kyr BP (Fig. 2). The sampling distance on the across flow transect ranged from one sample every 5 m for 195 m of Holocene ice and one sample every 7 m for 133 m of LGP ice. Samples were not directly drilled from the surface, but at a depth of 6–7 m to exclude dust and sediment from nearby moraines that may have settled on the glacier surface and contaminated the top several meters due to surface thermal cracking. The subsurface ice should not have been exposed after its initial

Table 1
Radiogenic isotope compositions of dust from Taylor Glacier ice samples. Sample names, strontium and neodymium isotopic compositions of ice core samples measured in this study, latitude, longitude, and approximate age based on a previously established timescale (Baggenstos, 2015) are noted. See Table S5 for radiogenic isotope compositions of Taylor Glacier soluble samples.

Sample ID	Latitude (S)	Longitude (E)	Approximate age (yr BP)	$^{87}Sr/^{86}Sr$	Sr ± 2σ 10^{-6}	ε_{Nd}	Nd ± 2σ (ε_{Nd})
N203	77°45.613′	161°43.424′	46,711	0.710785	38	−3.9	0.7
N196	77°45.612′	161°43.408′	44,374	0.709805	25	−2.4	0.5
N168	77°45.599′	161°43.360′	36,281	0.709407	41	0.1	0.3
N161	77°45.596′	161°43.349′	34,510	0.711300	86	−3.0	2.3
N147	77°45.592′	161°43.339′	30,080	0.709926	9	−3.3	0.6
N140	77°45.589′	161°43.311′	28,828	0.709370	37	−2.9	0.4
N133	77°45.586′	161°43.301′	26,820	0.708000	32	−1.6	0.2
N126	77°45.583′	161°43.286′	24,446	0.708870	47	−1.6	0.2
N119	77°45.580′	161°43.272′	21,891	0.708324	28	−1.5	0.2
N112	77°45.578′	161°43.277′	19,130	0.708144	45	−1.1	0.2
N105	77°45.574′	161°43.260′	17,138	0.710348	142	–	–
N98	77°45.562′	161°43.250′	16,116	0.708496	30	−1.4	0.4
N91	77°45.571′	161°43.238′	15,333	0.710151	27	−4.9	3.9
P20	77°45.528′	161°43.033′	16,035	–	–	−3.1	1.5
P40	77°45.487′	161°43.098′	14,491	0.7109740	40	−3.5	0.4
P60	77°45.511′	161°42.961′	13,588	0.711238	59	−3.0	0.9
P75	77°45.508′	161°42.943′	13,174	0.713714	117	–	–
P90	77°45.499′	161°42.912′	12,446	0.710207	24	−4.7	1.1
P110	77°45.493′	161°42.869′	11,609	0.710167	95	−4.6	0.7
P115	77°45.492′	161°42.861′	11,419	0.709306	63	–	–
P125	77°45.488′	161°42.848′	11,071	–	–	–	–
P130	77°45.486′	161°42.832′	10,927	0.711525	64	−2.3	0.8
P140	77°45.481′	161°42.820′	10,735	0.711879	111	−5.6	3.2
P145	77°45.479′	161°42.807′	10,557	0.710797	142	–	–
P155	77°45.475′	161°42.794′	10,259	0.707556	101	–	–
P165	77°45.471′	161°42.776′	10,082	–	–	–	–
P170	77°45.470′	161°42.768′	9980	0.711790	164	−5.0	4.3
P175	77°45.468′	161°42.757′	9864	0.712290	38	−4.1	1.1
P180	77°45.465′	161°42.753′	9722	–	–	–	–
P185	77°45.463′	161°42.750′	9587	0.712877	70	−7.8	3.2
P190	77°45.462′	161°42.728′	9458	0.713742	64	−1.1	1.3
P195	77°45.461′	161°42.719′	9351	0.713899	212	–	–
P200	77°45.457′	161°42.706′	9247	0.708625	120	−7.2	3.2
P205	77°45.455′	161°42.696′	9076	0.708355	58	−2.7	0.4
P210	77°45.455′	161°42.695′	8843	0.711243	61	1.9	2.2
P215	77°45.454′	161°42.687′	8725	0.711306	73	−2.4	3.4
R01	77°41.513′	160°57.849′	0	0.714944	65	−6.9	1.2
R01-D	77°41.513′	160°57.849′	0	0.714179	27	−3.5	1.2
N91-Surface	77°45.571′	161°43.238′	15,333	0.733621	32	−8.2	1.2

deposition as snow and subsequent transition into ice. Another potential phenomenon affecting the glacier surface is the concentration of morainal or dust material due to sublimation. To assess if surface contamination was present, we collected two samples of the same age (located at the same distance on the across flow transect). The first sample was collected at a depth of 6–7 m (following the sample protocol for all samples collected, sample name N91). A second sample was collected from superficial ice at a depth of 0–1 m (hereafter referred to as 'surface sample', sample name N91 surface). The surface sample and that at 6–7 m depth are the same age based on previous measurements showing that changes in ice age occur spatially across the ice flow (Aciego et al., 2007; Buizert et al., 2014). Two samples were collected at 6–7 m depth near Round Mountain, the accumulation-ablation transition zone (77°41′ S, 160°57′ E, Fig. 2). These samples are an approximation of zero-age ice (hereafter referred to as 'zero-age ice', sample names R01 and R01-D) due to their proximity to the equilibrium line at Taylor Glacier (Kavanaugh et al., 2009). None of the samples fractured during collection. Immediately after drilling and retrieval, the ice samples were cut in half with an electric chainsaw, and boxed and stored in an ice trench on site until transfer to McMurdo Station. Samples were then transported to the University of Michigan frozen.

3.2. Sample preparation and processing

Fourteen samples from the LGP (defined here as ~46-15 kyr BP time interval), 23 samples from the early Holocene (defined here as ~14.5–8.7 kyr BP time interval), and two 'zero-age' samples from Round Mountain (R01 and R01-D) were selected for analysis. The second zero-age sample (R01-D) was processed and measured separately to provide additional radiogenic isotope evidence for dust provenance. Trace and REE concentration and dust particle size distribution and concentration data were not obtained for sample R01-D. Each ~20 kg ice core sample was decontaminated and processed at the Glaciochemistry and Isotope Geochemistry Laboratory (GIGL) at the University of Michigan (UM). A longitudinal portion of each sample was cut using a custom-made stainless steel handsaw in a freezer at −15 °C for trace element (TE), REE, ion chromatography (IC, see Supplementary Information section S2.1), and Coulter® Counter analysis. The remaining portion of ice (for radiogenic isotope analysis) was decontaminated by sawing off the outer layer of the ice core and rinsing it with distilled ethanol prior to transfer into a custom-made acrylic ice core holder. The following sections describe specific sample handling procedures for different analyses.

3.3. Dust particle size and concentration analysis and dust flux calculations

The ice samples for dust concentration and size distribution analysis were triple-rinsed using MilliQ water with acid pre-cleaned low-density polyethylene (LDPE) pliers and stored in triple-rinsed polytetrafluoroethylene (PFTE) centrifuge tubes frozen until analysis following procedures described by Delmonte et al. (2004a). Approximately 20 mL were available for Coulter® Counter microparticle concentration and size distribution measurements in the diameter range of 0.6–17.9 μm. Each sample underwent five consecutive measurements. Blanks consisted of triple-rinsed PFTE centrifuge tubes filled with MilliQ water, and were negligible. The uncertainty for highly concentrated samples is <2% of the total concentration for 500,000 particles g^{-1}. Lower concentrated samples (from the Holocene) tend to experience some scattering (~2% for 1000 particles g^{-1}) (Delmonte et al., 2002). The dust flux rates at Taylor Glacier are determined by multiplying the variable water equivalent accumulation rates (calculated from ice equivalent) for each time period (Morse et al., 1998) by the dust concentrations (this study; see Table S4, Fig. 3a). We assume that all 0.6–17.9 μm particles measured by the Coulter® Counter are mineral dust.

3.4. Trace and rare earth element analysis

Ice core sections for TE and REE concentration analysis were triple-rinsed using MilliQ water and HNO_3 acid pre-cleaned LDPE pliers, and melted in pre-cleaned LDPE Nalgene bottles using procedures established by Boutron et al. (1990). The meltwater (containing both insoluble and soluble portion) was immediately acidified in 2% HNO_3 for approximately 1 month prior to analysis (procedural blanks are presented in Tables S1 and S2). Trace element (Li, Na, Al, V, Cr, Mn, Fe, Co, As, Rb, Sr, Nb, Ba, Bi, and U) and REE (La, Ce, Pr, Nd, Eu, Sm, Gd, Tb, Dy, Ho, Er, Tm, Yb, and Lu) concentrations were determined at The Ohio State University on a Thermo Element2 Inductively Coupled Plasma Sector Field Mass Spectrometer (ICP SFMS) coupled with a micro-flow nebulizer and a desolvation system (Apex Q). The system allows TE and REE detection down to the sub-pg g^{-1} levels (Gabrielli et al., 2006; Uglietti et al., 2014). For TEs, low mass resolution was used for the detection of Li, Na, Rb, Sr, Nb, Ba, Bi, and U, medium mass resolution for Al, V, Cr, Mn, Co, and high mass resolution for As.

3.5. Strontium and neodymium isotope analysis

After transport to ISO class 7 clean room at UM, the ice samples were rinsed with deionized water and melted using infrared radiation over a 24-h period, and the meltwater was immediately filtered through an acid-cleaned 0.2 μm Teflon filter. The filtrate (hereafter defined as the 'soluble fraction') was collected and dried down inside ISO class 4 laminar flow hood under nitrogen flow and infrared radiation before dissolution in 9 M HCl acid for ion-exchange column chemistry following the procedures of Aciego et al. (2009). The separated dust (hereafter defined as the 'insoluble fraction') was digested and dissolved directly off the 0.2 μm filters using HCl, aqua regia, and a concentrated HNO_3-dilute HF acid mixture, and subsequently dissolved in 9 M HCl acid. The samples were chemically separated using ion-exchange columns with Eichrom resins following previously established procedures (Aarons et al., 2016; Aciego et al., 2009) for Sr and Nd isotopic analysis.

After ion-exchange chemistry, chemically separated strontium (Sr) samples were measured on the UM Thermo Scientific Triton *Plus* Thermal Ionization Mass Spectrometer (TIMS) and normalized to $^{88}Sr/^{86}Sr = 8.375209$ to account for mass bias using the exponential law (Nier, 1938). Rubidium interferences were monitored by observing ^{85}Rb in the center cup, and all beam sizes were less than 10^{-13} A. The long-term reproducibility of Sr isotopic standard SRM987 (100 ng) is $^{87}Sr/^{86}Sr = 0.710256 \pm 8$ (2σ SD, n = 322). The United States Geologic Survey (USGS) reference material BCR-2 was measured concurrently with the Taylor Glacier samples and averaged 0.704999 ± 24 (2σ SD, n = 2), similar to published values (0.705000) (Jweda et al., 2015). The neodymium (Nd) samples were measured on a Thermo Scientific Triton *Plus* TIMS at the UM and normalized to $^{146}Nd/^{144}Nd = 0.7219$ using the exponential mass law and mass 149 was monitored for Sm interference. The long-term average for JNdi-1 is 0.512101 ± 24 (2σ SD, n = 19). The concurrently measured BCR-2 (10 ng) average is 0.512642 ± 21 (2σ SD, n = 4), close to the established measured values (0.512637) (Jweda et al., 2015). All Nd isotope compositions are reported here as ε_{Nd}, which is defined as: $\varepsilon_{Nd} = ([(^{143}Nd/^{144}Nd)_{sample}/(^{143}Nd/^{144}Nd)_{CHUR}]-1) \times 10^4$, where $(^{143}Nd/^{144}Nd)_{CHUR}$ is the Nd

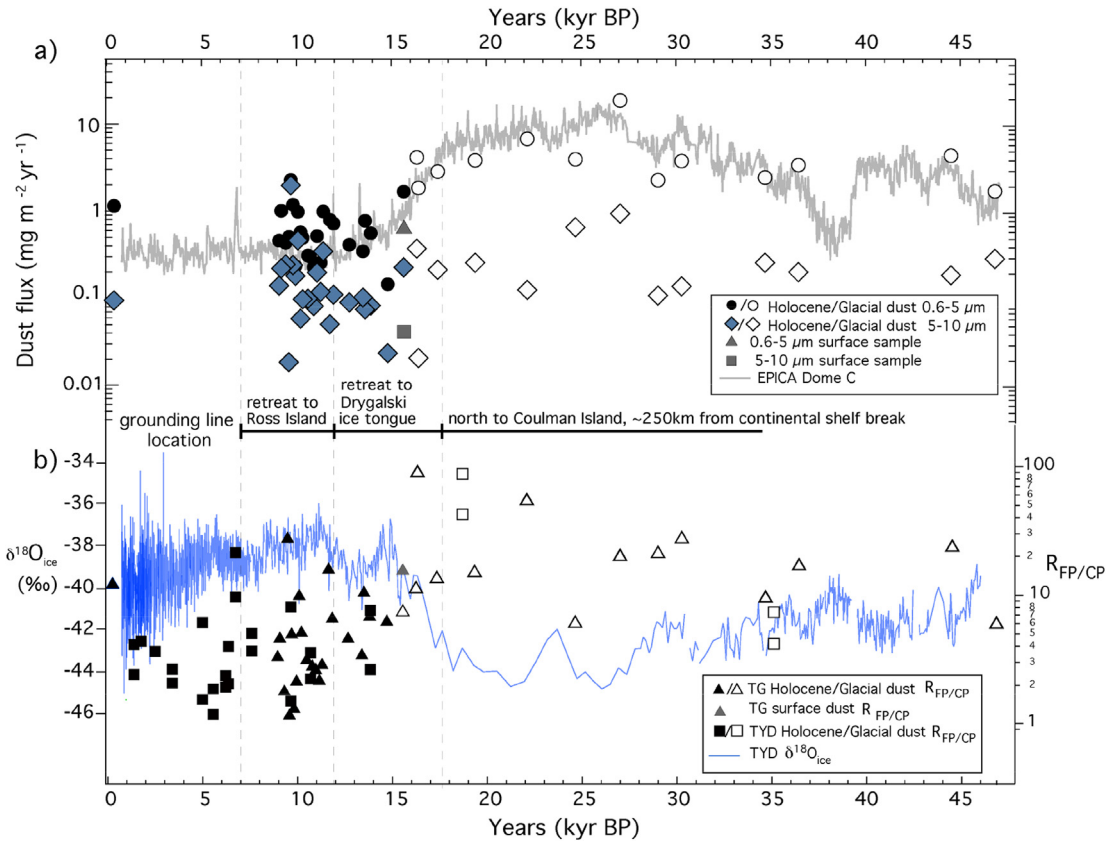

Fig. 3. Dust flux with respect to time and ratio of fine to coarse dust ($R_{FP/CP}$). a) Dust flux of Holocene and Glacial dust in 2 size fractions: 0.6–5 μm (black and white circles for Holocene and Glacial respectively) and 5–10 μm (teal and white diamonds for Holocene and Glacial respectively). A surface sample (N91 surface) is shown as gray triangle and square for 0.6–5 and 5–10 μm size fractions respectively. Also shown is dust flux from EDC (Lambert et al., 2012) (gray line). b) Ratio of fine (<5 μm) to coarse (5–10 μm) dust from Holocene and Glacial periods in Taylor Glacier samples (black and white triangles respectively), surface sample (gray triangle), and Taylor Dome ice core samples (black and white squares respectively) (Aarons et al., 2016). Also shown is the oxygen isotope composition of ice from the Taylor Dome ice core (blue line) (Steig et al., 2000) using the new age scale defined by Baggenstos (2015) and the approximate location of the Ross Ice Shelf grounding line (Licht et al., 1996; Conway et al., 1999). The timing of the Ross Ice Shelf evolution is based on ^{14}C ages of organic material incorporated within sediment cores from Licht et al. (1996) and Conway et al. (1999), with errors ranging from 45–610 and 50–97 years respectively. (For interpretation of the references to colour in this figure legend, the reader is referred to the web version of this article.)

isotopic composition of the Chondritic Uniform Reservoir (CHUR), which is $^{143}Nd/^{144}Nd = 0.512638$ (Jacobsen and Wasserberg, 1980).

4. Results

4.1. Dust concentration, flux, and size distribution

The dust concentrations of Taylor Glacier ice samples are generally higher during the LGP, with lower concentrations after the transition into the early Holocene (Fig. S1, Table S4). The Taylor Glacier dust exhibits a pattern similar to dust analyzed from the EPICA Dome C (EDC) ice core, higher during glacial periods and lower during interglacial periods, with dust ranging from 0.7 to 20 μm in diameter (Delmonte et al., 2004a). While dust concentrations reach over 1000 ppb during the LGP, they remain less than 100 ppb during the early Holocene. During the LGP, the concentration of fine fraction (0.6–5 μm diameter) dust closely resembles the EDC dust concentration. Meanwhile, the coarser Taylor Glacier dust (5–10 μm diameter) accounts for considerably less (a factor of 10 by number, nearly a factor of 100 by mass) of the total dust deposited at Taylor Glacier. Following the last deglaciation, the difference between fine and coarse dust concentration in the Taylor Glacier is smaller, suggesting that the input of coarser dust particles is larger in relative terms during the Holocene. The average fine to coarse concentration (by number) ratios during LGP and Holocene are 22 and 6 respectively, despite the lower total dust concentration during this time period. The surface sample, N91-surface (red symbols, Fig. S1), displays similar dust particle diameter and concentration with respect to the remaining Taylor Glacier samples. Dust particle diameter and concentration is a valuable tool for determining changes in dust sources and atmospheric pathways, and is discussed further below.

As dust is transported, coarse particles gravitationally settle out of the atmosphere first, resulting in finer particles with distance from the dust source area. The wind transport of dust is therefore size-specific, leading to well-sorted dust particle size distributions at distal deposition sites. In terms of particle size, the Holocene dust is not well sorted compared to the LGP dust, likely due to a shorter atmospheric transport time. The LGP dust exhibits lognormal size distributions with an average dust particle diameter of ~2 μm (Fig. S2), similar to findings for other ice cores from interior East Antarctica (Delmonte et al., 2002). As mentioned earlier, the relative input of coarse dust particles (>5 μm) to Taylor Glacier is higher during the Holocene compared to the LGP, which is also observed at Talos Dome, another coastal East Antarctic site located in the Ross Sea region (Albani et al., 2012; Delmonte et al., 2010, 2013). The presence of larger dust particles during the Holocene is not observed in ice cores from the Central East Antarctic Plateau (Delmonte et al., 2004b). The dust particle diameter data from Taylor Glacier during the Holocene is indicative of the influence of

local dust sources since larger dust particles will settle in close proximity to the source due to gravitational settling. It is possible that more vigorous atmospheric circulation at dust source areas (i.e. SSA) could result in coarser dust from remote sources deposited at Taylor Glacier, however this is unlikely based on the geochemical data (which suggests that input during the Holocene is originating from a likely combination of local and distal sources).

The average calculated dust flux of fine diameter particles in the Taylor Glacier during the LGP is 4.4 mg m^{-2} yr^{-1}, drastically dropping to 0.7 mg m^{-2} yr^{-1} in Holocene ice. For comparison, the average dust fluxes of coarser dust particles to Taylor Glacier during the LGP and Holocene were similar, at 0.3 and 0.2 mg m^{-2} yr^{-1} respectively. Overall, these trends in dust flux over the time period are similar for both EDC and the Taylor Glacier (Fig. 3a), suggesting that large-scale changes in dust transport occurring during major climate transitions are similar for both this interior East Antarctic site and for a coastal Antarctic site.

Changes in dust provenance can be discerned by comparing the relative input of fine versus coarse dust particles. For this work on the Taylor Glacier, we defined a parameter, $R_{FP/CP}$, which is the ratio of the concentration (in ppb) of fine dust (0.6–5 μm diameter) to coarse dust (5–10 μm diameter). We also include the $R_{FP/CP}$ parameter of samples from the Taylor Dome ice core (Aarons et al., 2016) to provide a more complete time series analysis (Fig. 3b). Similar to the dust concentration data, the $R_{FP/CP}$ parameter decreases significantly following the deglaciation, which occurred in Antarctica at 18.2 ± 0.7 kyr BP (Stenni et al., 2011). During the early Holocene, the Taylor Glacier record indicates large variability in the $R_{FP/CP}$ parameter with a generally decreasing trend. The $R_{FP/CP}$ parameter shows a higher relative input of fine particles during the LGP compared to the Holocene (Fig. 3b), which is also observed at Talos Dome (Albani et al., 2012) and within certain ice cores from the East Antarctic Plateau (Dome C and Komsomolskaia, Dronning Maud Land (EDML)) (Delmonte et al., 2004b; Wegner et al., 2015). Analysis of dust particle diameters from three east Antarctic ice cores (Dome C, Komsomolskaia, and Dome B) provides evidence of uniform dust input during the LGM; however, opposite regional trends occur during the transition between the LGP and the Holocene (Delmonte et al., 2004b). The differences in dust particle diameter input between Dome B and Dome C was attributed to differences in atmospheric transport pathways (i.e. horizontal trajectory or altitude of transport). During the Holocene, the wind speeds were likely weaker compared to the LGP, as steepened meridional temperature gradients during glacial periods lead to gustier conditions (McGee et al., 2010). Although the transport distance of dust to Taylor Glacier during the Holocene was probably shorter, it is possible that the weaker wind speeds resulted in finer dust transported from proximal sources. It is therefore important to examine changes in dust particle diameter together with additional geochemical parameters (e.g. radiogenic isotope composition, REE concentrations) to infer the cause of shifts in the $R_{FP/CP}$ parameter and the relationship to changes in dust source area and/or atmospheric transport mechanisms.

4.2. Trace and rare earth element concentration

Concentrations of TEs and REEs in Taylor Glacier ice during the LGP and the early Holocene are shown in Figs. S3 and 4 respectively. Distinct variations in concentrations are observed for all elements over the ~46,000 year time period studied here. Specific information regarding TE concentrations, which can provide insight into changes in dust and sea salt sources and strength, can be found in Text S1 in the Supporting Material.

The concentrations of REE are within the sub-pg g^{-1} to pg g^{-1} range, and large variation is observed among all samples. Ice samples from the Holocene (~0–14.5 kyr BP) exhibit lower REE concentrations than those from the LGP (~14.5–46.7 kyr BP). This difference in concentration is due to a higher dust input during glacial periods. The full range of REE concentrations is summarized in Table S2, and the REE concentrations (pg of element g^{-1} of ice) normalized to mean crustal REE abundance (pg of element g^{-1} of upper continental crust) (Wedepohl, 1995) are presented in Fig. 4. Here, comparable REE pattern shapes may be indicative of uniform dust source areas, or a congruent mixing of dust sources, whereas

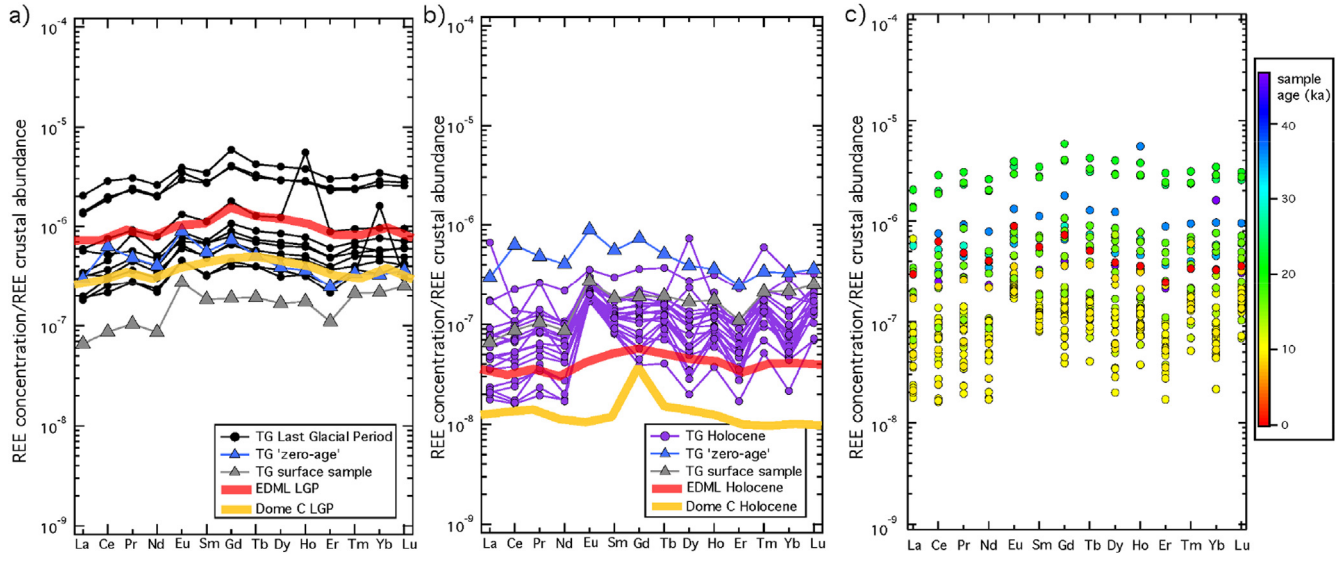

Fig. 4. Normalized rare earth element concentrations of Taylor Glacier dust in ice with respect to mean crustal abundance (Wedepohl, 1995). Taylor Glacier samples are separated by time periods: a) last glacial period, 'zero-age', and by location (surface sample). The normalized concentrations of rare earth elements from Dronning Maud Land (EDML) and EPICA Dome C (EDC) ice during the LGP (red and yellow solid lines respectively) are also shown (Gabrielli et al., 2010; Wegner et al., 2012). b) Holocene Taylor Glacier samples with 'zero-age' and surface sample, also shown are the normalized concentrations of rare earth elements from EDML and EDC ice during the Holocene (red and yellow solid lines respectively) (Gabrielli et al., 2010; Wegner et al., 2012). c) Rare earth element concentrations of Taylor Glacier ice throughout time period studied here (~46-0 kyr BP). Samples are colored based upon age, with blue being oldest and red being youngest. (For interpretation of the references to colour in this figure legend, the reader is referred to the web version of this article.)

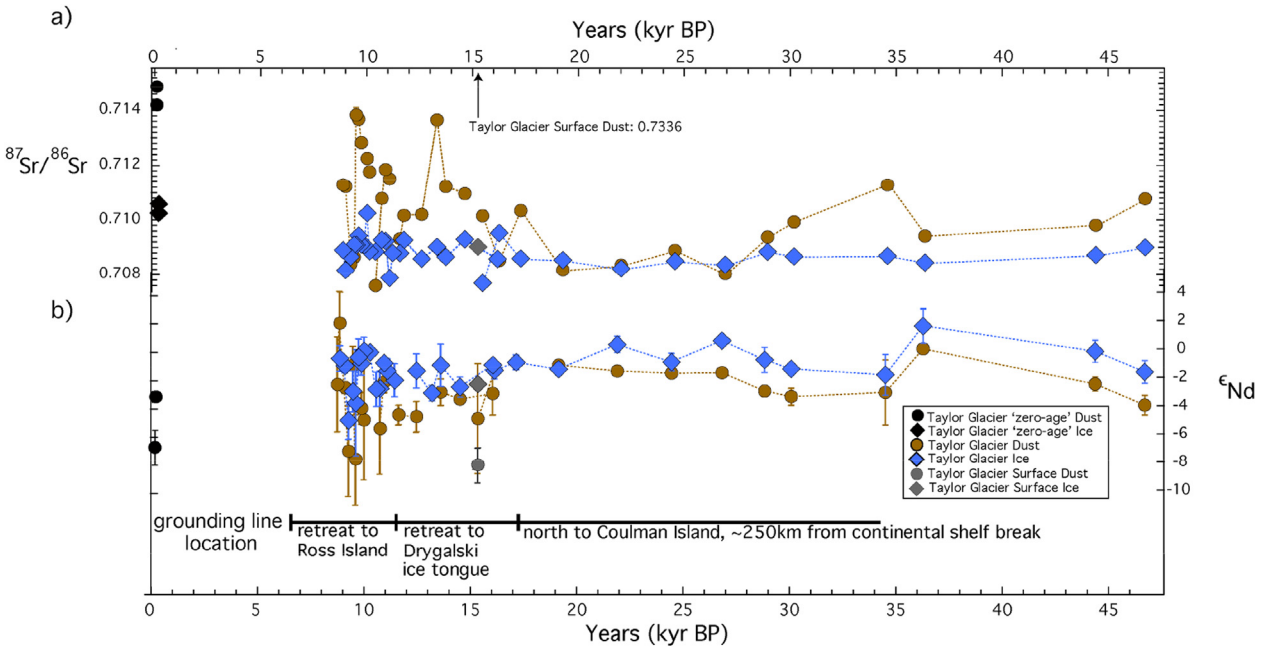

Fig. 5. Radiogenic isotopic composition of Taylor Glacier insoluble dust and ice throughout time. a) Strontium isotopic composition of Taylor Glacier dust (brown circles) and ice (blue diamonds). In many cases symbol size is larger than error bar. b) Neodymium isotopic composition of Taylor Glacier dust (brown circles) and ice (blue diamonds) along with Taylor Glacier surface sample dust (gray circle) and ice (gray diamond). Also shown is the description of the grounding line location of the Ross Ice Shelf. (For interpretation of the references to colour in this figure legend, the reader is referred to the web version of this article.)

variations from a constant pattern may be a result of a shift in dust source area. The observed REE patterns during the LGP are similar to concentrations observed in previous studies of Antarctic ice cores (Gabrielli et al., 2005, 2010; Wegner et al., 2012). Nearly all Holocene samples have a positive Eu anomaly (Fig. 4b) also observed in samples from the Taylor Dome ice core (Aarons et al., 2016), and some Holocene samples from EDML (Wegner et al., 2012), but is not found in ice cores from the interior East Antarctic ice sheet (Gabrielli et al., 2005, 2010). This may be indicative of similar dust sources transported to both EDML and Taylor Glacier during the Holocene, but not to other East Antarctic sites.

4.3. Radiogenic isotopic composition

Similar to radiogenic isotopes of dust (insoluble fraction) measured in ice from the Taylor Dome ice core, the early Holocene ice samples from this study span a broader range of Sr and Nd isotopic composition compared to the LGP ice (Aarons et al., 2016) (Fig. 5). The Taylor Glacier $^{87}Sr/^{86}Sr$ ratio ranges from 0.708000 to 0.711300 during the LGP, versus 0.707556–0.714944 during the early Holocene (Table 1, Fig. 5). The surface sample, 'N91 surface', is by far the most radiogenic with respect to Sr, at 0.733621 (Table 1, Fig. 5). The Nd isotopic compositions of LGP dust range from $\varepsilon_{Nd} = -3.9$ to 0.1, versus −8.2 to 1.9 during the early Holocene (Table 1, Fig. 5). The majority of insoluble early Holocene samples are more radiogenic with respect to Sr (median Holocene = 0.711274, median LGP = 0.709407), which has also been observed in ice from the Taylor Dome ice core (Aarons et al., 2016). The Nd isotopic composition becomes less radiogenic during the early Holocene (median Holocene $\varepsilon_{Nd} = -4.4$ versus median LGP = −2.4).

In comparison to the insoluble fraction of dust, the soluble particulate fraction (i.e. sea salt) exhibits more uniform Sr and Nd isotopic compositions (Table S5, Fig. 5). The average soluble Taylor Glacier $^{87}Sr/^{86}Sr$ ratio is 0.708577 during the LGP and 0.709023 during the early Holocene; both are close to the established modern seawater $^{87}Sr/^{86}Sr$ composition of 0.70917 (Hodell et al., 1990). The average soluble Taylor Glacier ε_{Nd} composition decreases following the transition from LGP to the early Holocene, shifting from −0.6 to −1.9.

For the most accurate characterization of dust sources, we include PSA data from the Southern Hemisphere; representing both long and short-range transport distance (Blakowski et al., 2016; Delmonte et al., 2013, 2010, 2004a; Gaiero, 2007). We consider PSA samples from the margin of the East Antarctic ice sheet in the Ross Sea Region, as well as samples from SSA to determine the relative contribution of local versus distal dust during the early Holocene. We also incorporate Australia in our coupled Sr-Nd isotope plot (Fig. 6), as this is a possible source of dust to the East Antarctic ice sheet (Revel-Rolland et al., 2006).

The combined Sr and Nd isotopic signatures of the samples vary based on sample age (Fig. 6). The LGP samples plot within the SSA source area, as specified by Delmonte et al. (2004a) and Gaiero (2007) (Fig. 6). The early Holocene samples are in general more radiogenic with respect to Sr, and suggest a mix of Ross Sea Sector potential source areas defined by Blakowski et al. (2016). The 'zero-age' samples have an even more Sr radiogenic signature, while the surface sample (N91-surface) plots far outside the range of either LGP or Holocene samples (Fig. 6a). Furthermore, the 'zero-age' sample also shows a distinct variation from the remainder of the Holocene REE concentrations, supporting the conclusion that the modern dust deposition at Taylor Glacier is different from both the LGP and Holocene.

The Sr and Nd isotopic composition of a surface sample (N91-surface) was used to assess the potential input of surface contaminating dust. Surface contaminating dust had a very radiogenic Sr dust composition (Fig. 5a). The Nd isotopic composition of surface dust (N91-surface) was considerably lower than subsurface ice of the same age (N91). The Sr-Nd isotopic composition of surface dust indicates that close range dust input (i.e. moraine material) to

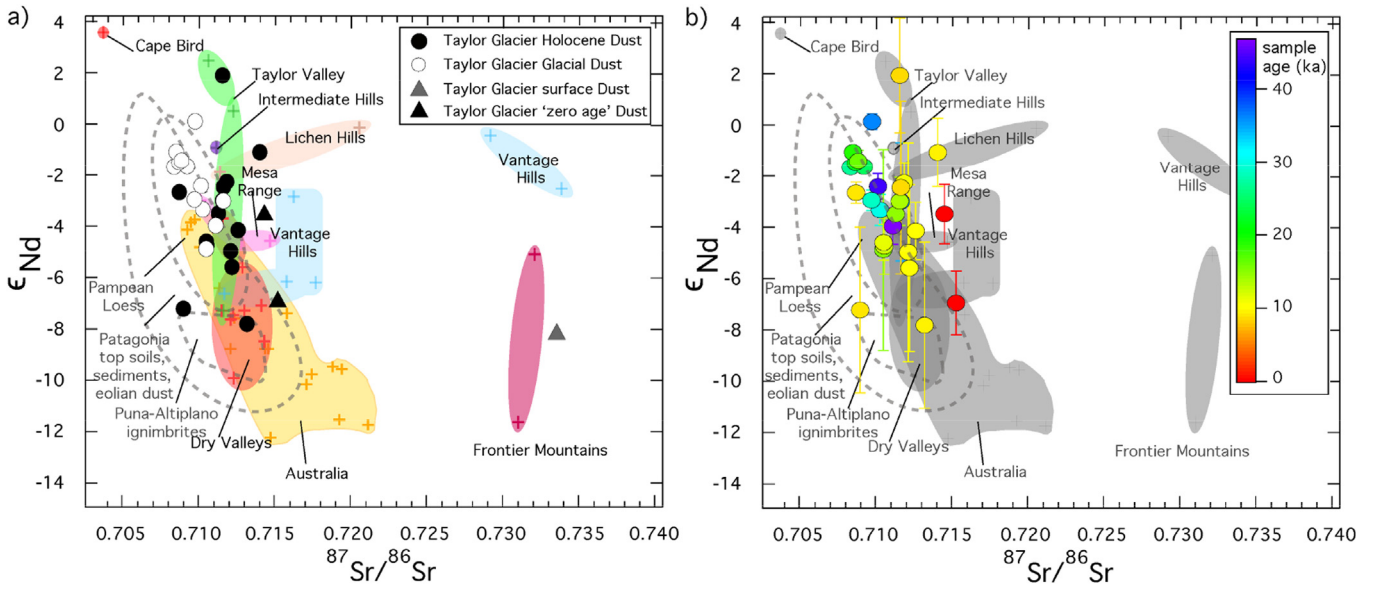

Fig. 6. Radiogenic isotopic compositions of Taylor Glacier ice core dust and potential source areas. a) Sr and Nd isotopic compositions of Taylor Glacier ice core dust from Holocene (black circles), Glacial dust (white circles), surface dust (gray diamond), and 'zero-age' dust (black triangles) with regional potential source areas plotted in various colors (colored crosses are individual data points) (Blakowski et al., 2016; Delmonte et al., 2013; Delmonte et al., 2010). Long-range potential source area of Southern South America is plotted within dashed gray lines (Delmonte et al., 2004a; Gaiero, 2007). b) Sr and Nd isotopic compositions of Taylor Glacier ice core dust from throughout time period studied here (~46-0 kyr BP). Samples are colored based upon age, with blue being oldest and red being youngest. Also shown in gray are regional and long-range potential source areas (Blakowski et al., 2016; Delmonte et al., 2013; Delmonte et al., 2010; Delmonte et al., 2004a; Gaiero, 2007). (For interpretation of the references to colour in this figure legend, the reader is referred to the web version of this article.)

Taylor Glacier does not diminish the isotopic signal of longer range transported dust (Fig. 6). It is unlikely that the surface contamination present in the surface sample (N91-surface) is coming directly from the Taylor Valley moraine material (77°39′ S, 162°54' E), which measures between $^{87}Sr/^{86}Sr = 0.710–0.712$ (Blakowski et al., 2016).

5. Discussion

Physical and chemical measurements of dust in ice cores are widely used to determine dust provenance (Basile et al., 1997; Delmonte et al., 2004a; Grousset et al., 1992; Vallelonga et al., 2010). In this work, we use these measurements to investigate whether some of the dust preserved within the Taylor Glacier was generated from a regional or proximal dust source area. In turn, these data can be extended to infer regional climate changes that occurred following the transition from the LGP to the early Holocene. We have characterized the Taylor Glacier dust by combining dust concentration and size distribution, REE concentrations, and Sr and Nd isotopic compositions to gain the most comprehensive understanding of dust sources, transport pathways, and inferred changes in atmospheric conditions. Additionally, chloride and sea salt sodium (ssNa) concentration measurements of the Taylor Glacier ice (see Supplementary Material for analytical methods and discussion) provide further insight into ice chemistry changes with respect to the opening of the Ross Sea. High chloride and ssNa concentrations in Taylor Glacier ice are observed following the retreat of the Ross Ice Shelf and increase in sea salt source strength. The higher concentration of chloride and ssNa compared to Taylor Dome ice is most likely a result of this coastal proximity (Fig. S4).

The Ross Ice Shelf retreat would have likely been driven by changes in global oceanic circulation and ambient temperatures, and we use the $\delta^{18}O_{ice}$ composition from Taylor Dome (Steig et al., 2000) as a climate proxy for data comparison. The isotopic composition of oxygen in H_2O in the ice ($\delta^{18}O_{ice}$) has been used as an indicator of air temperature at the ice core deposition site (Jouzel et al., 1997). The $R_{FP/CP}$ parameter (Fig. 3b) provides insight into dust particle size deposited on Taylor Glacier, and this is a reflection of distance to source and wind strength. We examine these two parameters together to explore the relationship between climate shifts, Ross Ice Shelf retreat, and dust variation.

5.1. Dust provenance during the last glacial period and deglaciation

The $\delta^{18}O_{ice}$ at Taylor Dome (Steig et al., 2000) (Fig. 3b) is contemporaneous with the stages of the Ross Ice Shelf retreat. The $\delta^{18}O_{ice}$ composition during the LGP is low (between −44 and −40‰) and is generally decreasing until after the LGM, when it begins to rise rapidly at ~17 kyr BP. During this $\delta^{18}O_{ice}$ increase at ~17 kyr BP, the $R_{FP/CP}$ values of dust particles remain high until ~15.5 kyr BP (Fig. 3b). A negative correlation between Taylor Glacier dust particle size and $\delta^{18}O_{ice}$ composition (Fig. 3b), illustrates the link between background dust flux and large-scale temperature changes (Lambert et al., 2008). During the LGP, the $\delta^{18}O_{ice}$ is low, and the $R_{FP/CP}$ value remains high; whereas, following the deglaciation, the $\delta^{18}O_{ice}$ is higher, and the $R_{FP/CP}$ value decreases (Fig. 3b). The relationship between the timing of changes in the Taylor Glacier dust particle size and a proxy for temperature ($\delta^{18}O_{ice}$) provides further evidence that changes in dust sources and transport pathways are likely to coincide with large-scale climate shifts.

Fig. 4c illustrates the REE concentrations of Taylor Glacier ice, and samples are color-coded according to age. REE compositions clearly vary based on their age: REE concentrations are high in samples from the LGM whereas REE concentrations are lower in samples from the LGP (>35 kyr BP). The REE patterns for the Taylor Glacier samples are temporally invariable throughout the LGP (Fig. 4a), which is indicative of one predominant source of dust or alternatively a constant mix of several different sources. These Taylor Glacier REE patterns are very similar to observed REE patterns from interior East Antarctic ice cores such as EDML and EDC

(Gabrielli et al., 2010; Wegner et al., 2012), suggesting that the sources and atmospheric pathways of dust to both interior East Antarctica (EDML and EDC) and coastal sites (Taylor Dome and Taylor Glacier) during the LGP remain similar, despite their considerable distance from each other.

As for Sr and Nd isotopic compositions, all dust samples from LGP ice plot within or at the margin of the source area designation for SSA (Fig. 6), the dominant source of dust to East Antarctica during this time period (Delmonte et al., 2010, 2004a, 2004b). Close examination of variations in Sr and Nd isotope composition based on sample age during the LGP reveals trends related to the time of deposition not discernible in REE patterns. The oldest samples from the LGP (Fig. 6b) span between $-3.9 < \varepsilon_{Nd} < 0.1$ and $0.709926 < {}^{87}Sr/{}^{86}Sr < 0.711300$. This large isotopic range suggests that the LGP dust is originating from more than one source, possibly from SSA, as well as from local Ross Sea Sector PSAs. In contrast, the samples from the LGM (26.8–19.1 kyr BP) (Fig. 6b) are tightly clustered together between $-1.6 < \varepsilon_{Nd} < -1.1$ and $0.708000 < {}^{87}Sr/{}^{86}Sr < 0.708870$, similar to results from EDC (Delmonte et al., 2008), indicating a singular, uniform source region (SSA). Finally, ice samples from the deglaciation and into the early Holocene (coinciding with the time period of ~18.2–8.7 kyr BP) (Fig. 6b) span a broad range in Sr and Nd isotope composition: $-7.8 < \varepsilon_{Nd} < 1.9$ and $0.708355 < {}^{87}Sr/{}^{86}Sr < 0.713742$. Based on this large variation it is likely that dust from this time period originates from a mixture of two or more sources (SSA and McMurdo Sound are possible source areas).

5.2. New dust source(s) during the Holocene

The dust flux (Fig. 3a) to Taylor Glacier and EDC are markedly similar, specifically in the fine fraction (0.6–5 μm) of Taylor Glacier dust. There is a time period of exclusion (~10-9 kyr BP), where the dust flux is higher in the Taylor Glacier; however, the primary significance of the Taylor Glacier record is that larger dust particles comprise more of the total dust input during the Holocene. The higher input of large dust particles during the Holocene may be indicative of a change in dust source area/distance. The higher local input during this time period (supported by both dust particle size and geochemical data) could be attributed to a shift in atmospheric transport mechanisms (i.e. an alteration in storm trajectories and/or dominant weather pathways as hypothesized in Morse et al. (1998)). This hypothesis is supported by the change in dust provenance discussed below.

The timing of the climate shifts recorded in the $\delta^{18}O_{ice}$ record and retreat in the Ross Ice Shelf is a reflection of the strong relationship between changes in ice cover and temperature on a hemispheric scale. The timing of the Ross Ice Shelf retreat is supported by the ssNa and Cl^- concentration data, which vary based on the opening of the Ross Sea (Fig. S4). The Ross Ice Shelf retreat occurred at the same time as the shifts in dust particle size variation in the Taylor Glacier record (Fig. 3b), and the correlation between $R_{FP/CP}$ ratios and $\delta^{18}O_{ice}$ composition illustrates that dust sources and transport pathways at this coastal East Antarctic site are linked to the rapid retreat of the Ross Ice Shelf precipitated by large-scale temperature changes.

The REE concentrations gradually decrease with respect to decreasing age, excluding the zero-age sample (R01), which has a higher REE concentration and a REE pattern similar to samples from ~15 to 10 kyr BP. The majority of samples from the early Holocene display a positive Eu anomaly (Fig. 4b) observed in the Taylor Dome ice core record (Aarons et al., 2016) and some Holocene samples from EDML (Wegner et al., 2012), although the anomaly is not present in EDC (Gabrielli et al., 2010). Previous work by Wegner et al. (2012) characterizing the REE concentration patterns of Antarctic PSA samples from the ice-free areas within the Dry Valleys, New Zealand and SSA showed that all three areas had an Eu anomaly. The positive Eu anomaly is also found in young volcanic source area dust from Patagonia (Gaiero et al., 2004). The presence of an Eu anomaly in the Taylor Glacier ice may be attributed to the mixing of dust originating from both local sources and a constant baseline input of long range transported dust (e.g. SSA). The Holocene REE patterns of interior East Antarctic (EDC) ice is very different than the Taylor Glacier (this study) and Taylor Dome ice (Aarons et al., 2016), suggesting differences in dust provenance related to the coastal proximity of the ice core locations. However, the previous work by Wegner et al. (2012) identified a strong Eu anomaly in 24 Holocene samples from EDML, which may be evidence of locally (Antarctic) derived dust input to both EDML and Taylor Glacier.

A significant portion (7 out of 17 samples) of coupled Sr and Nd isotope compositions for our early Holocene dust are not entirely constrained to the observed SSA array (Fig. 6). The Eu anomaly appears consistently in the REE concentration patterns of the Holocene samples from Taylor Glacier, and indicates that the dust deposited on Taylor Glacier during the early Holocene could originate from SSA and local Ross Sea sector dust sources. The 'surface sample' (N91-surface) also has a positive Eu anomaly, which may imply that Ross Sea Sector sources can be attributed to dust input to the Taylor Glacier during the Holocene. The 'surface sample' (N91-surface) is similar in REE pattern to the majority of the Holocene samples from Taylor Glacier (Fig. 4a and b); thus, early Holocene samples at Taylor Glacier may also be originating from local dust sources.

The early Holocene samples span a broad range of Sr ($0.707556 < {}^{87}Sr/{}^{86}Sr < 0.714944$) and Nd ($-8.2 < \varepsilon_{Nd} < -1.9$) isotope compositions and are most likely a mixture of previously identified Ross Sea Region dust sources (Blakowski et al., 2016) and dust from SSA. Dust from PSAs throughout the Ross Sea Region and Victoria Land span more radiogenic compositions with respect to Sr, up to 0.750 in Northern Victoria Land (Delmonte et al., 2010), and dust from the McMurdo Sound region is more radiogenic with respect to Nd, ε_{Nd} up to 7.0 (Blakowski et al., 2016). Although dust from the Ross Sea Region overlaps with PSA dust from more remote Southern Hemisphere sources in Sr and Nd isotopic composition, the additional geochemical and physical characterization of Taylor Glacier dust (dust concentration and size distribution, TE and REE compositions) is supportive of a dust input from a mixture of local areas during the early Holocene. Previous research geochemically characterizing PSAs from Victoria Land and the McMurdo Sound sector noted that the majority these PSAs have been ice-free and exposed to wind erosion during glacial and interglacial periods due to the extremely arid environmental conditions (Blakowski et al., 2016). Therefore, it is unlikely that deglacial exposure of local dust sources is contributing to dust input changes at Taylor Glacier.

5.3. A new source of dust to Antarctica?

Southern South America has been attributed as the primary source of dust to East Antarctica during the LGP and the Holocene (Basile et al., 1997; Delmonte et al., 2004a; Gaiero, 2007; Grousset et al., 1992; Vallelonga et al., 2010). However, Revel-Rolland et al. (2006) noted that glacial Sr and Nd isotopic compositions of dust in East Antarctic ice overlaps with dust originating from the Australian Lake Eyre Basin. Vallelonga et al. (2010) then excluded Australian PSAs as a major contributor of dust to Antarctica during the LGP on the basis of ${}^{208}Pb/{}^{207}Pb$ isotope compositions. The fine fraction of Australian PSAs are more radiogenic with respect to ${}^{208}Pb/{}^{207}Pb$ compared to the majority of Pb isotope signatures identified in LGP samples from EDC ice (Vallelonga et al., 2010).

Recent work by Gili et al. (2016) used Pb isotope data to confirm that SSA is the main contributor of dust to East Antarctica during the LGP and the Holocene; however, both SSA and Australia may be mixing end-members. There are several interglacial dust $^{208}Pb/^{207}Pb$ compositions from EDC that overlap with the Australian PSA compositional trend, and in this study Holocene samples from Taylor Glacier plot within the Australian Sr-Nd compositional trend (Fig. 6). Therefore Australia cannot be entirely excluded as a potential contributor of dust during the Holocene.

In addition to radiogenic isotopes, the physical properties of dust particles can aid in determining changes in provenance and transport distance. The relationship between $R_{FP/CP}$ and Sr and Nd isotope composition in Taylor Glacier samples is not linear (Fig. S5), suggesting that changes in the observed isotopic compositions are a result of changes in dust provenance rather than grain-size related fractionation (see Supplementary Information section S3.1). One of our 'zero-age' samples, R01, has a $R_{FP/CP}$ value higher than the majority of Holocene samples (Fig. 3b), indicating that the dust originates from a more distal source. The 'zero-age' sample (R01) also does not have a pronounced positive Eu anomaly found in other samples from the early Holocene (Fig. 4a and b). This supports the suggestion that dust sources may have changed from local input during the early Holocene to a more distal source (i.e. input from SSA and Australia) during the late Holocene. The $^{87}Sr/^{86}Sr$ ratios of samples R01 and R01-D are more radiogenic than all other samples (Figs. 5a and 6), excluding the surface sample, N91-surface. The Nd isotopic composition of R01 is distinctly negative, plotting on the periphery of the remaining early Holocene samples cluster (Figs. 5b and 6), whereas R01-D is more positive and may be comprised of a dust mixture from more than one source (i.e. Australia, SSA, and/or Northern Victoria Land).

When viewed in the context of the Sr-Nd isotope plot of Southern Hemisphere PSA's (Fig. S6) sample R01 plots within the established Australian source area (Delmonte et al., 2004a; Revel-Rolland et al., 2006), also suggesting that Australia cannot be excluded as a possible dust source to East Antarctica during the Holocene. In addition, satellite images and back trajectory modeling demonstrate that air masses from Australia circumnavigate Antarctica, indicating that there is potential for Australian dust deposition in Antarctica (De Deckker et al., 2010). The observed $^{87}Sr/^{86}Sr$ and ε_{Nd} isotope compositions for Australian dust span from 0.709 to 0.732 and from −3 to −15, respectively (Revel-Rolland et al., 2006), and samples R01 and R01-D are within those boundaries ($^{87}Sr/^{86}Sr$ = 0.714944, 0.714179 and ε_{Nd} = −6.9, −3.5). The Sr and Nd isotopic compositions are quite variable and the recent input of Australian dust to East Antarctica is consistent with only one combined Sr-Nd data point. Therefore, it is not possible to conclude with certainty the provenance of late-Holocene dust sources and suggests future work should address this late Holocene change in dust provenance.

6. Conclusions

Our combined physical and chemical analyses of Taylor Glacier ice provide the first multi-millennial record of dust input to a coastal East Antarctic site during a full transition from the LGP to the early Holocene. The increased number of samples facilitates observation of temporal changes in REE concentrations and radiogenic isotope composition throughout the LGP, deglaciation, and early Holocene. The dust concentrations, particle size distribution, REE concentrations, and isotopic compositions of Taylor Glacier ice suggest a shift in dust source provenance following the deglaciation. It is likely that dust sources to Taylor Glacier have changed from SSA during the LGP to local Ross Sea Sector with input partially originating from SSA during the early Holocene. The dust transport pathways are possibly still evolving/variable, as a 'zero-age' sample appears uniquely different than the other early Holocene samples. The retreat in the Ross Ice Shelf is strongly correlated with temperature at the ice core location site ($\delta^{18}O_{ice}$ composition), and the study shows that changes in local dust inputs occur at approximately the same time (to the extent that they are known) as the stages of Ross Ice Shelf retreat. Future recession of the ice shelf and a retreat of the ice sheet margin may result in higher input of local dust sources as evidenced from the change of local atmospheric circulation patterns surrounding Taylor Glacier (Morse et al., 1998). To resolve the primary and secondary sources of dust during the Holocene, it would be beneficial to characterize more Antarctic PSAs in larger size fractions, as this would have an effect upon observed isotopic compositions. A cross-disciplinary, multi-proxy approach to determine dust sources transported to Antarctica both in the ice core record along with modern collection techniques can provide further insight into environmental changes occurring both in the past and future. The potential of increasing Australian dust input to Antarctica during the Holocene due to amplified dust availability at the source area(s) is worthy of further investigation in future ice core studies.

Acknowledgements

This work was funded by grants from the Rackham Graduate School and the Turner Award from the Department of Earth and Environmental Sciences at the University of Michigan to S.M. Aarons and from NSF OPP Antarctic Glaciology Award 1246702 to S.M. Aciego and P. Gabrielli. We thank M. Jayred for drilling assistance, D. Baggenstos for support with the age scale, and M. Grieman and two anonymous reviewers for helpful comments on the manuscript.

Appendix A. Supplementary data

Supplementary data related to this article can be found at http://dx.doi.org/10.1016/j.quascirev.2017.03.011.

References

Aarons, S.M., Aciego, S.M., Gabrielli, P., Delmonte, B., Koornneef, J.M., Wegner, A., Blakowski, M.A., 2016. The impact of glacier retreat from the Ross Sea on local climate: characterization of mineral dust in the Taylor Dome ice core, East Antarctica. Earth Planet. Sci. Lett. 444, 34–44.

Aciego, S.M., Bourdon, B., Lupker, M., Rickli, J., 2009. A new procedure for separating and measuring radiogenic isotopes (U, Th, Pa, Ra, Sr, Nd, Hf) in ice cores. Chem. Geol. 266, 194–204.

Aciego, S.M., Cuffey, K.M., Kavanaugh, J.L., Morse, D.L., Severinghaus, J.P., 2007. Pleistocene ice and paleo-strain rates at Taylor Glacier, Antarctica. Quat. Res. 68, 303–313.

Albani, S., Delmonte, B., Maggi, V., Baroni, C., Petit, J.R., Stenni, B., Mazzola, C., Frezzotti, M., 2012. Interpreting last glacial to Holocene dust changes at Talos dome (East Antarctica): implications for atmospheric variations from regional to hemispheric scales. Clim. Past 8, 741–750.

Baggenstos, D., 2015. Taylor Glacier as an Archive of Ancient Ice for Large-volume Samples: Chronology, Gases, Dust, and Climate, Earth Sciences. University of California, San Diego, Ann Arbor, MI, p. 148.

Basile, I., Grousset, F.E., Revel, M., Petit, J.R., Biscaye, P.E., Barkov, N.I., 1997. Patagonian origin of glacial dust deposited in East Antarctica (Vostok and Dome C) during glacial stages 2, 4 and 6. Earth Planet. Sci. Lett. 146, 573–589.

Biscaye, P., Grousset, F., Revel, M., Van der Gaast, S., Zielinski, G., Vaars, A., Kukla, G., 1997. Asian provenance of glacial dust (stage 2) in the Greenland Ice Sheet project 2 ice core, Summit, Greenland. J. Geophys. Res. 102, 765–781.

Bauska, T.K., 2013. Carbon Cycle Variability during the Last Millennium and Last Deglaciation. Oregon State University.

Blakowski, M.A., Aciego, S.M., Delmonte, B., Baroni, C., Salvatore, M.C., Sims, K.W.W., 2016. Sr-Nd-Hf isotope characterization of dust source areas in Victoria land and the McMurdo sound sector of Antarctica. Quat. Sci. Rev. 141, 26–37.

Bliss, A.K., Cuffey, K.M., Kavanaugh, J.L., 2011. Sublimation and surface energy budget of Taylor Glacier, Antarctica. J. Glaciol. 57, 684–696.

Boutron, C.F., Patterson, C.C., Barkov, N.I., 1990. The occurrence of zinc in Antarctic ancient ice and recent snow. Earth Planet. Sci. Lett. 101, 248–259.

Buizert, C., Baggenstos, D., Jiang, W., Purtschert, R., Petrenko, V.V., Lu, Z.T., Muller, P., Kuhl, T., Lee, J., Severinghaus, J.P., Brook, E.J., 2014. Radiometric Kr-81 dating identifies 120,000-year-old ice at Taylor Glacier, Antarctica. Proc. Natl. Acad. Sci. U. S. A. 111, 6876–6881.

Conway, H., Hall, B.L., Denton, G.H., Gades, A.M., Waddington, E.D., 1999. Past and future grounding-line retreat of the West Antarctic ice sheet. Science 286, 280–283.

De Deckker, P., Norman, M., Goodwin, I.D., Wain, A., Gingele, F.X., 2010. Lead isotopic evidence for an Australian source of aeolian dust to Antarctica at times over the last 170,000 years. Palaeogeogr. Palaeoclimatol. Palaeoecol. 285, 205–223.

Delmonte, B., Andersson, P., Hansson, M., Schoberg, H., Petit, J.-R., Basile-Doelsch, I., Maggi, V., 2008. Aeolian dust in East Antarctica (EPICA - Dome C and Vostok): provenance during glacial ages over the last 800 kyr. Geophys. Res. Lett. 35 http://dx.doi.org/10.1029/2008GL033382.

Delmonte, B., Baroni, C., Andersson, P.S., Narcisi, B., Salvatore, M.C., Petit, J.-R., Scarchilli, C., Frezzotti, M., Albani, S., Maggi, V., 2013. Modern and Holocene aeolian dust variability from Talos Dome (Northern Victoria Land) to the interior of the Antarctic ice sheet. Quat. Sci. Rev. 64, 76–89.

Delmonte, B., Baroni, C., Andersson, P.S., Schoberg, H., Hansson, M., Aciego, S., Petit, J.R., Albani, S., Mazzola, C., Maggi, V., Frezzotti, M., 2010. Aeolian dust in the Talos Dome ice core (East Antarctica, Pacific/Ross Sea sector): Victoria land versus remote sources over the last two climate cycles. J. Quat. Sci. 25, 1327–1337.

Delmonte, B., Basile-Doelsch, I., Petit, J., Maggi, V., Revel-Rolland, M., Michard, A., Jagoutz, E., Grousset, F., 2004a. Comparing the EPICA and Vostok dust records during the last 220,000 years: stratigraphical correlation and provenance in glacial periods. Earth-Sci. Rev. 66, 63–87.

Delmonte, B., Petit, J.R., Andersen, K.K., Basile-Doelsch, I., Maggi, V., Ya Lipenkov, V., 2004b. Dust size evidence for opposite regional atmospheric circulation changes over East Antarctica during the last climatic transition. Clim. Dyn. 23, 427–438.

Delmonte, B., Petit, J.R., Maggi, V., 2002. Glacial to Holocene implications of the new 27000-year dust record from the EPICA Dome C (East Antarctica) ice core. Clim. Dyn. 18, 647–660.

EPICA Community Members, 2004. Eight glacial cycles from an Antarctic ice core. Nature 429 (6992), 623–628.

Gabrielli, P., Barbante, C., Turetta, C., Marteel, A., Boutron, C., Cozzi, G., Cairns, W., Ferrari, C., Cescon, P., 2006. Direct determination of rare earth elements at the subpicogram per gram level in antarctic ice by ICP-SFMS using a desolvation system. Anal. Chem. 78 (6), 1883–1889.

Gabrielli, P., Planchon, F.A.M., Hong, S., Lee, K.H., Hur, S.D., Barbante, C., Ferrari, C.P., Petit, J.R., Lipenkov, V.Y., Cescon, P., Boutron, C.F., 2005. Trace elements in Vostok Antarctic ice during the last four climatic cycles. Earth Planet. Sci. Lett. 234, 249–259.

Gabrielli, P., Wegner, A., Petit, J.R., Delmonte, B., De Deckker, P., Gaspari, V., Fischer, H., Ruth, U., Kriews, M., Boutron, C., Cescon, P., Barbante, C., 2010. A major glacial-interglacial change in aeolian dust composition inferred from rare earth elements in Antarctic ice. Quat. Sci. Rev. 29, 265–273.

Gaiero, D.M., 2007. Dust provenance in Antarctic ice during glacial periods: from where in southern South America? Geophys. Res. Lett. 34 http://dx.doi.org/10.1029/2007GL030520.

Gaiero, D.M., Depetris, P.J., Probst, J.-L., Bidart, S.M., Leleyter, L., 2004. The signature of river-and wind-borne materials exported from patagonia to the southern latitudes: A view from REEs and implications for paleoclimatic interpretations. Earth Planet. Sci. Lett. 219, 357–376.

Gili, S., Gaiero, D.M., Goldstein, S.L., Chemale Jr., F., Koester, E., Jweda, J., Vallelonga, P., Kaplan, M.R., 2016. Provenance of dust to Antarctica: a lead isotopic perspective. Geophys. Res. Lett. 43, 2291–2298.

Grousset, F.E., Biscaye, P.E., 2005. Tracing dust sources and transport patterns using Sr, Nd and Pb isotopes. Chem. Geol. 222, 149–167.

Grousset, F.E., Biscaye, P.E., Revel, M., Petit, J.-R., Pye, K., Joussaume, S., Jouzel, J., 1992. Antarctic (Dome C) ice-core dust at 18 k.y. B.P.: isotopic constraints on origins. Earth Planet. Sci. Lett. 111, 175–182.

Hammer, C., Clausen, H., Dansgaard, W., Neftel, A., Kristinsdottir, P., Johnson, E., 1985. Continuous impurity analysis along the dye-3 deep core. Geophys. Monogr. Ser. 33, 90–94.

Hodell, D.A., Mead, G.A., Mueller, P.A., 1990. Variation in the strontium isotopic composition of seawater (8 Ma to present): implications for chemical weathering rates and dissolved fluxes to the oceans. Chem. Geol. 80, 291–307.

Jacobsen, S.B., Wasserberg, G.J., 1980. Sm-Nd isotopic evolution of chondrites. Earth Planet. Sci. Lett. 50, 139–155.

Jouzel, J., Alley, R., Cuffey, K., Dansgaard, W., Grootes, P., Hoffmann, G., Johnsen, S., Koster, R., Peel, D., Shuman, C., Stievenard, M., Stuiver, M., White, J., 1997. Validity of the temperature reconstruction from water isotopes in ice cores. J. Geophys. Res. Oceans 102, 26471–26487.

Jweda, J., Bolge, L., Class, C., Goldstein, S.L., 2015. High Precision Sr-Nd-Hf-Pb isotopic compositions of USGS reference material BCR-2. Geostand. Geoanal. Res. 40, 101–115.

Kavanaugh, J.L., Cuffey, K.M., Morse, D.L., Bliss, A.L., Aciego, S.M., 2009. Dynamics and mass balance of Taylor Glacier, Antarctica: 3. State of mass balance. J. Geophys. Res. Earth Surf. 114 http://dx.doi.org/10.1029/2009JF001331.

Kuhl, T.W., Johnson, J.A., Shturmakov, A.J., Goetz, J.J., Gibson, C.J., Lebar, D.A., 2014. A new large-diameter ice-core drill: the blue ice drill. Ann. Glaciol. 55 http://dx.doi.org/10.3189/2014AoG68A009.

Lambert, F., Delmonte, B., Petit, J.R., Bigler, M., Kaufmann, P.R., Hutterli, M.A., Stocker, T.F., Ruth, U., Steffensen, J.P., Maggi, V., 2008. Dust-climate couplings over the past 800,000 years from the EPICA Dome C ice core. Nature 452, 616–619.

Lambert, F., Bigler, M., Steffensen, J.P., Hutterli, M.A., Fischer, H., 2012. Centennial mineral dust variability in high-resolution ice core data from Dome C, Antarctica. Clim. Past 609–623.

Licht, K.J., Jennings, A.E., Andrews, J.T., Williams, K.M., 1996. Chronology of late Wisconsin ice retreat from the western Ross Sea, Antarctica. Geology 24, 223–226.

Loulergue, L., Schilt, A., Spahni, R., Masson-Delmotte, V., Blunier, T., Lemieux, B., Barnola, J.M., Raynaud, D., Stocker, T.F., Chappellaz, J., 2008. Orbital and millenial-scale features of atmospheric CH4 over the past 800,000 years. Nature 453, 383–386.

Lüthi, D., Le Floch, M., Bereiter, B., Blunier, T., Barnola, J.M., Siegenthaler, U., Raynaud, D., Jouzel, J., Fischer, H., Kawamura, K., Stocker, T.F., 2008. High-resolution carbon dioxide concentration record 650,000-800,000 years before present. Nature 453, 379–382.

Marino, F., Castellano, E., Ceccato, D., De Deckker, P., Delmonte, B., Ghermandi, G., Maggi, V., Petit, J.R., Revel-Rolland, M., Udisti, R., 2008. Defining the geochemical composition of the EPICA Dome C ice core dust during the last glacial-interglacial cycle. Geochem. Geophys. Geosystems 9. http://dx.doi.org/10.1029/2008GC002023.

McGee, D., Broecker, W.S., Winckler, G., 2010. Gustiness: The driver of glacial dustiness? Quat. Sci. Rev. 29, 2340–2350.

Morse, D.L., 1997. Glacier Geophysics at Taylor Dome. University of Washington, Antarctica.

Morse, D.L., Waddington, E.D., Steig, E.J., 1998. Ice age storm trajectories inferred from radar stratigraphy at Taylor Dome, Antarctica. Geophys. Res. Lett. 25, 3383–3386.

Nier, A.O., 1938. The isotopic constitution of strontium, barium, bismuth, thallium and mercury. Phys. Rev. 5, 275–279.

Petit, J.R., Jouzel, J., Raynaud, D., Barkov, N.I., Barnola, J.M., Basile, I., Bender, M., Chappellaz, J., Davis, M., Delaygue, G., Delmotte, M., Kotlyakov, V.M., Legrand, M., Lipenkov, V.Y., Lorius, C., Pepin, L., Ritz, C., Saltzman, E., Stievenard, M., 1999. Climate and atmospheric history of the past 420,000 years from the Vostok ice core, Antarctica. Nature 399, 429–436.

Petit, J.R., Delmonte, B., 2009. A model for large glacial-interglacial climate-induced changes in dust and sea salt concentrations in deep ice cores (central Antarctica): palaeoclimatic implications and prospects for refining ice core chronologies. Tellus Ser. B 61, 768–790.

Petrenko, V.V., Severinghaus, J.P., Schaefer, H., Smith, A.M., Kuhl, T., Baggenstos, D., Hua, Q., Brook, E.J., Rose, P., Kulin, R., Bauska, T., Harth, C., Buizert, C., Orsi, A., Emanuele, G., Lee, J.E., Brailsford, G., Keeling, R., Weiss, R.F., 2016. Measurements of 14C in ancient ice from Taylor Glacier, Antarctica constrain in situ cosmogenic 14CH4 and 14CO production rates. Geochim. Cosmochim. Acta 107, 62–77.

Reeh, N., Oerter, H., Letreguilly, A., Miller, H., Hubberten, H.-W., 1991. A new, detailed ice-age oxygen-18 record from the ice-sheet margin in central west Greenland. Glob. Planet. Change 4, 373–383.

Revel-Rolland, M., De Deckker, P., Delmonte, B., Hesse, P., Magee, J., Basile-Doelsch, I., Grousset, F., Bosch, D., 2006. Eastern Australia: a possible source of dust in East Antarctica interglacial ice. Earth Planet. Sci. Lett. 249, 1–13.

Steig, E.J., Morse, D.L., Waddington, E.D., Stuiver, M., Grootes, P.M., Mayewski, P., Twickler, M.S., Whitlow, S., 2000. Wisconsinan and Holocene climate history from an ice core at Taylor Dome, western Ross Embayment, Antarctica. Geogr. Ann. 82A, 213–235.

Stenni, B., Buiron, D., Frezzotti, M., Albani, S., Barbante, C., Bard, E., Barnola, J.M., Baroni, M., Baumgartner, M., Bonazza, M., Capron, E., Castellano, E., Chappellaz, J., Delmonte, B., Falourd, S., Genoni, L., Iacumin, P., Jouzel, J., Kipfstuhl, S., Landais, A., Lemieux-Dudon, B., Maggi, V., Masson-Delmotte, V., Mazzola, C., Minster, B., Montagnat, M., Mulvaney, R., Narcisi, B., Oerter, H., Parrenin, F., Petit, J.R., Ritz, C., Scarchilli, C., Schilt, A., Schupbach, S., Schwander, J., Selmo, E., Severi, M., Stocker, T.F., Udisti, R., 2011. Expression of the bipolar see-saw in Antarctic climate records during the last deglaciation. Nat. Geosci. 4, 46–49.

Sugden, D.E., McCulloch, R.D., Bory, A.J.M., Hein, A.S., 2009. Influence of Patagonian glaciers on Antarctic dust deposition during the last glacial period. Nat. Geosci. 2, 281–285.

Uglietti, C., Gabrielli, P., Olesik, J.W., Lutton, A., Thompson, L.G., 2014. Large variability of trace element mass fractions determined by ICP-SFMS in ice core samples from worldwide high altitude glaciers. Appl. Geochem. 47, 109–121.

Vallelonga, P., Gabrielli, P., Balliana, E., Wegner, A., Delmonte, B., Turetta, C., Burton, G., Vanhaecke, F., Rosman, K.J.R., Hong, S., Boutron, C.F., Cescon, P., Barbante, C., 2010. Lead isotopic compositions in the EPICA Dome C ice core and southern hemisphere potential source areas. Quat. Sci. Rev. 29, 247–255.

Wedepohl, K.H., 1995. The composition of the continental crust. Geochim. Cosmochim. Acta 59, 1217–1232.

Wegner, A., Fischer, H., Delmonte, B., Petit, J.R., Erhardt, T., Ruth, U., Svensson, A., Vinther, B., Miller, H., 2015. The role of seasonality of mineral dust concentration and size on glacial/interglacial dust changes in the EPICA dronning maud land ice core. J. Geophys. Res. Atmos. 120, 9916–9931.

Wegner, A., Gabrielli, P., Wilhelms-Dick, D., Ruth, U., Kriews, M., De Deckker, P., Barbante, C., Cozzi, G., Delmonte, B., Fischer, H., 2012. Change in dust variability in the Atlantic sector of Antarctica at the end of the last deglaciation. Clim. Past 8, 135–147.